

www.acsaem.org Article

# A Facile Polymer Interlayer for Lithium Stability in Lithium—Sulfur Batteries

Taber Yim, Rhyz Pereira, Neal Cardoza, and Vibha Kalra\*



Cite This: ACS Appl. Energy Mater. 2023, 6, 12326-12333



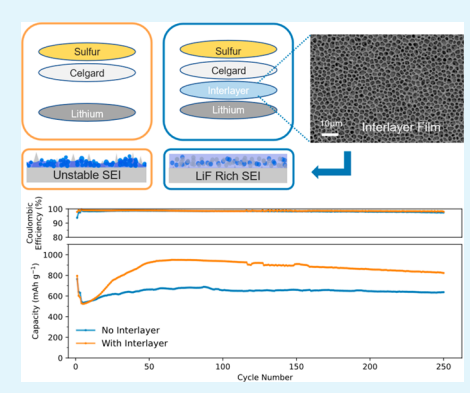
**ACCESS** 

III Metrics & More

Article Recommendations

s Supporting Information

**ABSTRACT:** Lithium—sulfur (Li—S) batteries are a promising next-generation battery chemistry, but the challenges that surround lithium metal anodes prevent it from being realized as a commercial technology. In this work, we address lithium stability via a facile, 5 μm thin PVDF—HFP and LiNO<sub>3</sub> interlayer placed directly on the lithium anode. We created the interlayer with a simple blade casting technique that was performed under ambient conditions. It was then studied in Li—Li symmetric cells, showing stability through 500 h. Using post-mortem XPS, we found that a robust solid electrolyte interface with increased LiF content was formed in situ from the interlayer materials. This provided heightened stability compared to conventional cells without the interlayer. Additionally, we investigated the synergistic effect of the interlayer materials. Finally, using this interfacial layer in a Li—S coin cell battery provided a capacity of 858 mAh g<sup>-1</sup> at 200 cycles, an increase of 32% compared to conventional Li—S cells without the interfacial layer. This work represents a step toward the stability of lithium metal anodes and their viability in commercial batteries.



KEYWORDS: Li-S batteries, lithium stability, interlayer, SEI, PVDF-HFP, lithium nitrate

#### 1. INTRODUCTION

Batteries with higher energy density are being sought to meet the demand from electric vehicles in a society that is continually being electrified. Lithium-ion batteries (LIBs) are a mature technology but are reaching their theoretical capacity threshold. Therefore, lithium sulfur batteries (LSBs) are an attractive battery technology due to their 8-fold increase in theoretical capacity (1675 mAh g $^{-1}$ ) compared to LIBs. Other benefits of LSBs include the affordability of sulfur at \$100/ton, its natural abundance, and its low environmental impact. <sup>1</sup>

Like other lithium metal batteries (LMBs), LSBs suffer from lithium instability due to lithium's high reactivity, dendrite growth, the formation of a dead lithium layer, and an unstable solid electrolyte interface (SEI). During cycling, the anode experiences volume changes that break the SEI. This SEI instability means that the electrolyte will continually deplete as it reacts further with the exposed, fresh lithium anode. The consequential nonuniform lithium deposition leads to dendrite growth. These dendrites can also become detached from the anode in the following cycles, a process that generates the dead lithium layer. Collectively, these issues exacerbate each other and result in poorly performing LSBs. Furthermore, if the dendrite growth becomes too severe, the battery will short circuit in a dangerous, rapid discharging event. Unsolved, these issues prevent commercialization of LMBs.

To address the issue of lithium metal stability, many techniques have been employed in previous works. <sup>5</sup> Aurbach et al. studied the effect of lithium salts such as lithium

bis(trifluoromethane)sulfonamide (LiTFSI) and lithium nitrate (LiNO<sub>3</sub>). They found that these salts were beneficial in the formation of SEI components such as lithium fluoride (LiF) and lithium oxide (Li<sub>2</sub>O). LiF has since become a wellstudied SEI component. However, Li et al. found that dendrite growth is not fully suppressed by the insufficient LiF generated from the LiTFSI in commercial electrolytes. Zu et al. investigated electrolyte additives that contained metal ions (such as copper, gold, or silver) with lower reactivity with sulfur compared to lithium. These metal ions lowered the crystallinity of impurity phases, stabilizing the anode. Sparingly solvating electrolytes are also of interest because the solvent molecules will coordinate with lithium salts rather than react with the lithium anode. Additionally, polymer electrolytes have become popular recently. They offer many advantages over traditional liquid electrolyte systems but still have issues to resolve, such as low ionic conductivity at room temperature. 10 Nevertheless, they do offer the ability to physically suppress dendrite growth and incorporate beneficial filler molecules. Ex-situ lithium surface modification is another technique that allows for greater control over the SEI

Received: August 22, 2023
Revised: November 13, 2023
Accepted: November 14, 2023
Published: December 7, 2023





compounds. For example, Guo et al. coated lithium metal with a solution of poly(vinylidene fluoride-co-hexafluoropropylene) (PVDF–HFP), dimethyl sulfoxide (DMSO), and N,N-dimethylformamide (DMF) that yielded a LiF-rich layer upon drying. Thao et al. achieved a similar result using poly(vinylidene fluoride) (PVDF). In-situ SEI manipulation was achieved by Dong et al. using magnesium nitride (Mg<sub>3</sub>N<sub>2</sub>) as an electrolyte additive. During cycling, Mg<sub>3</sub>N<sub>2</sub> plated on the lithium metal and was reduced to form lithium nitride (Li<sub>3</sub>N), another beneficial SEI component. While there are numerous methods to approach lithium stability, industrial adoption of a technique would likely require the use of commercially available and well-studied materials, preferably processed in a simple manner.

Herein, we demonstrate heightened lithium stability using a facile 5  $\mu$ m thin polymer interlayer. It was composed solely of PVDF–HFP and LiNO<sub>3</sub> and created in natural, ambient conditions. We show that LiF was formed in situ during cycling, creating a robust SEI from the two constituent interlayer components. Using post-mortem XPS, we found the interlayer provided a level of LiF in the SEI that was more effective compared to a conventional cell without it. We also investigated the synergistic effect between the two interlayer materials. Overall, this work represents a step toward industry-friendly technology advancement.

#### 2. EXPERIMENTAL SECTION

- **2.1. Materials.** Polyacrylonitrile (PAN,  $M_{\rm w}=150000~{\rm g~mol}^{-1}$ ), N,N- dimethylformamide (DMF, 99.8%), and poly(vinylidene fluoride)-co-hexafluoropropylene (PVDF–HFP,  $M_{\rm w}\sim40000$  and  $M_{\rm n}\sim130000$ ) were purchased from Sigma-Aldrich. Commercial ether electrolyte (dimethoxyethane:1,3-dioxolane 1:1 by volume with 1 M lithium bis(trifluoromethane)sulfonamide and 1 wt % lithium nitrate (DME:DOL 1:1 vol % with 1 M LiTFSI and 1 wt % LiNO<sub>3</sub>)) was purchased from Gotion. Sulfur (99.5%, sublimed, 100 mesh) and lithium (99.9%, 250  $\mu$ m thick, 15.6 mm diameter) were purchased from Alfa Aesar. Acetone (99.5%) was purchased from VWR. Trilayer commercial battery separators (Celgard 2325) were purchased from Celgard.
- **2.2. Cathode Fabrication.** Cathodes for Li–S cells were produced by carbonizing electrospun PAN nanofibers. The precursor electrospinning solution was 10 wt % PAN in DMF. An 8.5 kV potential was applied at a distance of 15.25 cm. Fibers were spun to create a layered mat. The mat was stabilized in an oven (Binder FD 23) at 280 °C. The stabilized fibers were then pyrolyzed in a tube furnace (MTI GSL-1100X-S) under constant nitrogen flow at 1000 °C for 60 min. The pyrolyzed fibers were cut into 11 mm diameter disks, and sulfur was incorporated via melt diffusion in a heat press at 318 °F. The amount of sulfur in the cathode was 1 mg, and the average sulfur loading for all cathodes was about 1.0 mg cm<sup>-2</sup>. Electrolyte was added at an E/S ratio of 20 (E = microliters of electrolyte, S = milligrams of sulfur).
- **2.3. Interlayer Fabrication.** The interlayer between the Celgard separator and the anode was made from a precursor solution with varying weight percentages of PVDF–HFP and LiNO<sub>3</sub> in acetone. The solution was stirred at 50 °C for 4 h until homogeneous. The solution was cast on a glass plate to obtain film thicknesses of 5–25  $\mu$ m with a doctor blade using an automatic coater (MTI MSK-AFA-II). The casting was done outside of the glovebox. Once casted, the film was immediately transferred to a vacuum oven and dried for 24 h without the use of heat. Once dry, the film was cut and punched into 19 mm diameter circles. Interlayers hereafter will be referred to by their compositional ratio of polymer (P) to lithium nitrate (N). For example, an interlayer with a composition of 2 parts PVDF–HFP to 1 part LiNO<sub>3</sub> will be termed 2P:1N.
- **2.4. Coin-Cell Fabrication.** Cathodes were transferred to an argon-filled glovebox (MBraun LABstar, O<sub>2</sub> and H<sub>2</sub>O levels <1 ppm).

The Li–S coin cells were fabricated using CR2032 casings (MTI and Xiamen TMAX Battery Equipment, China), circular lithium anodes, a Celgard 2325 separator, an interlayer when being used, and Gotion commercial ether electrolyte. Once all components were aligned, the cell was sealed with an electronic crimper (MTI MSK-160D). The assembled coin cells were rested at room temperature and open circuit voltage for 12 h before initiating electrochemical experiments. Symmetric coin cells were assembled with bare lithium metal for each electrode (each 250  $\mu \rm m$  thick). The separator was either Celgard 2325 or a 25  $\mu \rm m$  polymer film made of the interlayer materials. The amount of commercial ether electrolyte added was 15  $\mu \rm L$ . The interlayer material was tested as a 25  $\mu \rm m$  stand-alone separator so it could be compared directly to the 25  $\mu \rm m$  Celgard separator. Symmetric cells were rested for 2 h before testing.

- **2.5. Electrochemical Characterization.** Li–S coin cell galvano-static cycling tests were performed on a battery cycler (Neware BTS 4000 or Maccor Series 4000) with a cycling profile of 2 cycles at C/10 and 2 cycles at C/5, followed by extended cycling at C/2 (1C = 1672 mAh g<sup>-1</sup> sulfur) between 1.8 and 2.6 V. Cyclic voltammetry (CV) was performed on a potentiostat (Biologic VMP3) at a scan rate of 0.5 mV s<sup>-1</sup> between 1.8 and 2.6 V with respect to Li/Li<sup>+</sup>. Electrochemical impedance spectroscopy (EIS) was conducted on a Biologic potentiostat from 1 MHz to 100 mHz with a 10 mV potential amplitude. Symmetric cells were cycled with an energy density of 1 mA cm<sup>-2</sup> and a capacity of 1 mAh cm<sup>-2</sup>. Dynamic symmetric cell cycling was performed with a profile of 2 cycles at 0.5 mA cm<sup>-2</sup>, followed by 10 cycles each of 1, 2, and 4 mA cm<sup>-2</sup>, followed by 5 cycles of 5 mA cm<sup>-2</sup>, and finally extended cycling at 1 mA cm<sup>-2</sup>.
- **2.6. Material Characterization.** The morphology of the polymer interlayer was observed by using a scanning electron microscope (SEM, Zeiss Supra 50VP). The bond signatures of polymer film samples were collected with a Fourier transform infrared spectrometer (FTIR, Nicolet iS50, Thermo-Fisher Scientific) using an extended range attenuated total reflection (ATR) diamond. The chemical environment of lithium anode surfaces was analyzed with postmortem X-ray photoelectron spectroscopy (XPS, PHI VersaProbe 5000). During XPS studies, coin cells with an interlayer were sputtered for 30 min using an argon milling process to probe closer to the lithium surface, rather than the interlayer surface. CasaXPS (ver. 23.19PR1.0) software was used for spectra analysis.

#### 3. RESULTS AND DISCUSSION

3.1. Interlayer Characterization. The SEM images for the 2P:1N and 3P:1N interlayers show a uniform pore morphology on the surface of the polymer films that extends through the depth of the film. The pore sizes for the 2P:1N interlayer ranged from about 0.5–3  $\mu$ m (Figure 1a). Figure 1b illustrates the interconnected pore structure of the interlayer where pores do not extend directly through the entire height of the film but do exist throughout it. The mechanism by which the pores form is believed to be via water vapor depositing on the surface of the polymer as it dries. By using acetone, a fastevaporating solvent in ambient conditions, the local temperature near the polymer film decreases and facilitates water condensation. The polymer reorganizes around the water droplet to form honeycomb-like pores. 14 Based on SEM observations of the interlayer, there were no large lithium salt crystals or polymer agglomerates. The pore size and distribution were beneficial in this study because they allowed the interlayer to uptake liquid electrolyte easily. Figure 1c shows the morphology of the 3P:1N interlayer. Here, we observed a denser polymer matrix. It also had an interconnected pore structure (Figure 1d).

Figure 2 shows the FTIR spectra of a PVDF–HFP polymer film with and without the LiNO<sub>3</sub> salt. The peaks at 839 cm<sup>-1</sup> and 1429 cm<sup>-1</sup> are unique to the  $\beta$ -phase of PVDF–HFP. The peak at 1400 cm<sup>-1</sup> is characteristic of the  $\alpha$ -phase of PVDF–

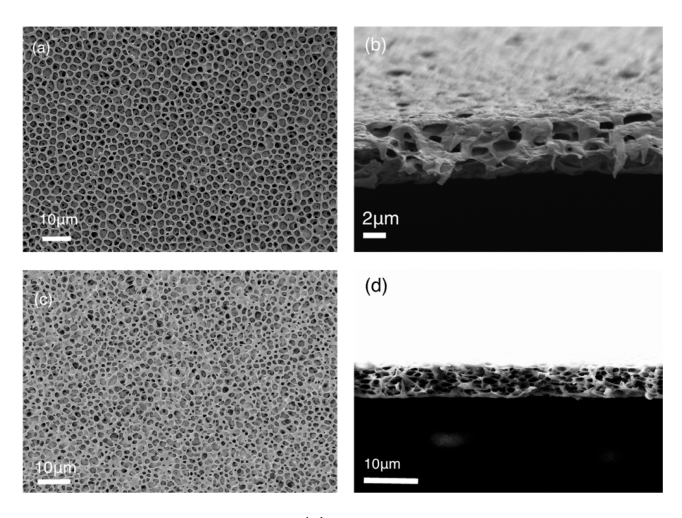


Figure 1. SEM image of (a) the 2P:1N interlayer at  $1000 \times$  magnification (10  $\mu$ m scale bar); (b) cross section of the 2P:1N interlayer at 3000× magnification (2  $\mu$ m scale bar); (c) 3P:1N at 1000× magnification (10  $\mu$ m scale bar); and (d) cross section of the 3P:1N interlayer at 1500× magnification (10  $\mu$ m scale bar).

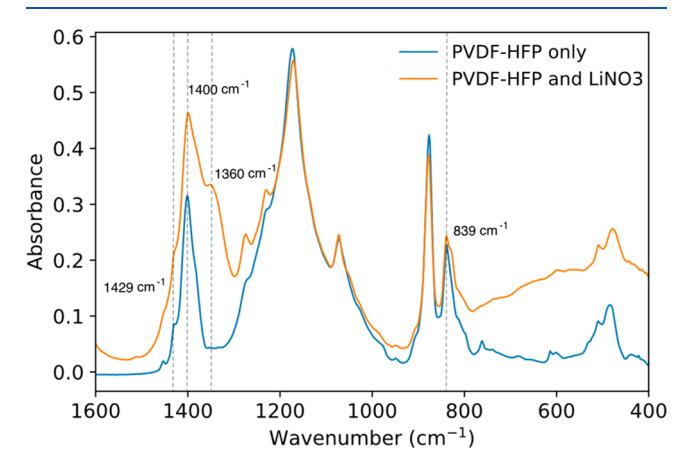


Figure 2. FTIR spectrum comparing a PVDF–HFP polymer film with and without  ${\rm LiNO_3}$ .

HFP. <sup>15</sup> In the sample with LiNO<sub>3</sub>, there is a peak at 1360 cm<sup>-1</sup>, which is the typical region of the nitrate ion. <sup>16</sup> The superposition of both spectra shows that no major peaks are shifted or lost. The absence of major peak shifting indicates that the lithium salt does not interfere with the polymer structure. In the spectrum that includes LiNO<sub>3</sub>, the region from around 800 cm<sup>-1</sup> to 400 cm<sup>-1</sup> is not as clear as the spectrum without the nitrate. This is because LiNO<sub>3</sub> is hygroscopic and creates some water interference.

**3.2. Electrochemical Evaluation.** To investigate how the different films affect lithium stability, they were tested as a gel polymer electrolyte (GPE) in Li–Li symmetric cells. Figure 3a shows a comparison of PVDF–HFP GPEs with and without the addition of LiNO<sub>3</sub>. As shown, the polarization voltage in the cell with LiNO<sub>3</sub> was stable for hundreds of hours with the voltage initially steady at around 23 mV and then slowly minimizing to around 18 mV. The cell without LiNO<sub>3</sub> had a much higher and more unstable polarization, with a voltage ranging from 39 to over 110 mV. We hypothesize that the presence of LiNO<sub>3</sub> facilitates the formation of LiF, leading to greater stability. This could be due to the oxidative nature of LiNO<sub>3</sub> which could help decompose PVDF–HFP, helping it

react with the lithium metal. The commercial ether electrolyte already contains some amount of LiNO<sub>3</sub>, but the additional LiNO<sub>3</sub> in the interlayer heightens the effect and further stabilizes the lithium anode. The effect may be more pronounced because the LiNO<sub>3</sub> in the interlayer is held in very close proximity to the lithium anode rather than in the liquid electrolyte. Furthermore, LiNO<sub>3</sub> itself reacts with lithium to form Li<sub>2</sub>O<sub>2</sub> a favorable SEI component.<sup>6</sup>

Figure 3b shows a comparison among Celgard, a 2P:1N GPE, and a 3P:1N GPE, which are all 25  $\mu$ m in thickness. The plot shows the symmetric cell response to a dynamic current profile initially, followed by constant current cycling. The plot shows the highest polarization for the Celgard cell at all current rates. At 5C rate cycles, the 3P:1N GPE showed the lowest polarization at around 50 mV compared to around 95 mV for the 2P:1N GPE. They were both much lower than the Celgard cell, which showed polarization spikes over 200 mV (Figure 3c). Additionally, the voltage profiles for each cycle in the Celgard cell were extremely uneven compared to those of the GPEs made from the interlayer materials. This indicates that the plating and stripping of lithium in the Celgard cell was much more resistive. 17 During the extended cycling, the Celgard cell initially decreased in polarization but rapidly grew. By contrast, the 2P:1N and 3P:1N GPEs maintained a relatively even polarization curve for several hundred hours with minimal polarization (Figure 3d). The higher polarization and uneven voltage profiles exhibited by the Celgard cell were likely caused by thick dead lithium layers that build up on the electrodes and a less robust SEI. Our hypothesis for the 3P:1N GPE performing better than the 2P:1N GPE is that there is a denser polymer network that physically inhibits dendrite growth and the growth of the dead lithium layer, thus lowering the polarization in the cell. This is seen in the SEM images (Figure 1a,c).

The EIS plot provides insight into the SEI and charge transfer resistances in the cell (Figure 4). 18,19 The first semicircle represents the SEI resistance and was smaller initially in the 2P:1N interlayer coin cell compared with the Celgard cell, possibly because the interlayer has additional LiNO<sub>3</sub>. The additional LiNO<sub>3</sub> is in close proximity to the anode and likely creates additional NO<sub>3</sub><sup>-</sup> ions as it dissociates, increasing lithium ion conductivity. 20 However, the interlayer cell showed a larger second semicircle, indicating a larger charge transfer resistance. This is likely due to the presence of a polymer layer. After 50 cycles, the charge transfer resistances of both cells decreased. Part of the reason this happens may be due to the rearrangement of the sulfur active material, which is electronically insulating. 21,22 Initially, sulfur was heat pressed into the CNF cathode. Upon cycling, sulfur begins to redistribute itself to the most electronically active sites. Redistribution can occur when polysulfides redeposit in the cathode, helping disperse sulfur more evenly throughout the cathode. Ultimately, the resistance drops because there is now a finer, homogeneous distribution of sulfur on conductive carbon. After 50 cycles, in the interlayer cell, the charge transfer resistance was no longer greater than that in the Celgard cell. This may be because the polymer interlayer had enough time to be fully wetted with electrolyte. The SEI resistance also dropped, which may be because the SEI had ample time to fully develop. The resistances of both cells were similar after 50 cycles, which shows that the thin and conductive interlayer did not detrimentally affect the lithium-sulfur coin cell.

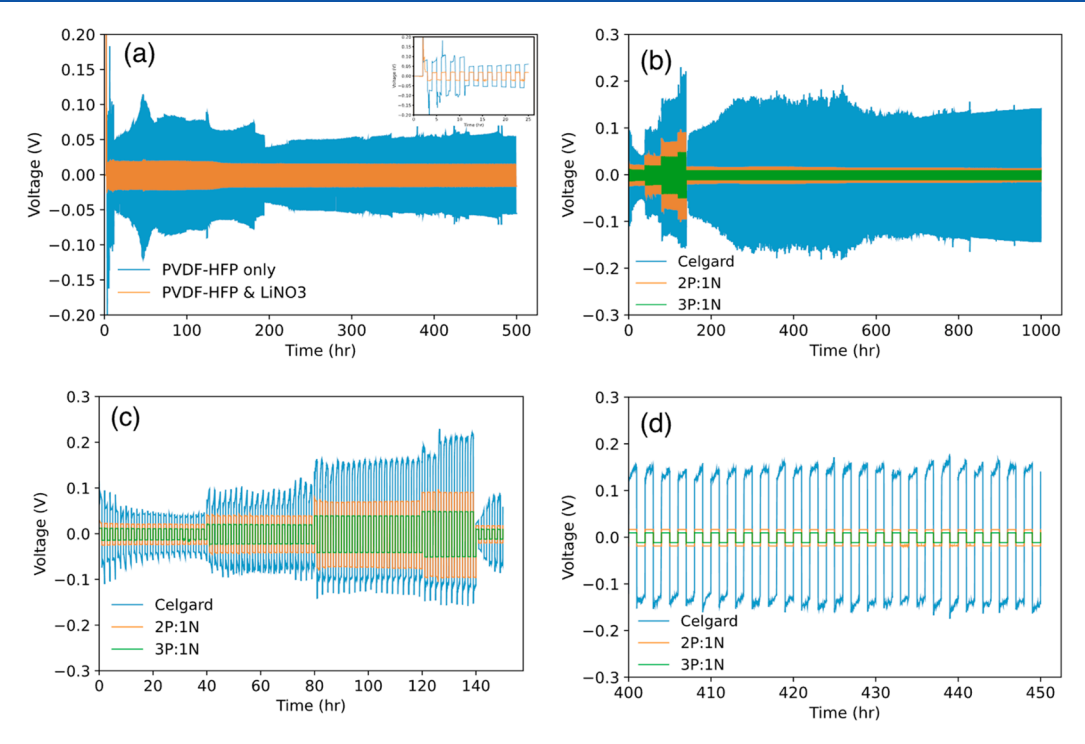


Figure 3. (a) Li–Li symmetric cells comparing PVDF–HFP GPEs with and without LiNO<sub>3</sub>, inset showing cycles 0–25. Dynamic cycling profile for Li–Li symmetric cells comparing Celgard and 2P:1N and 3P:1N separators at (b) 0–1000 h, (c) 0–150 h, and (d) 400–450 h.

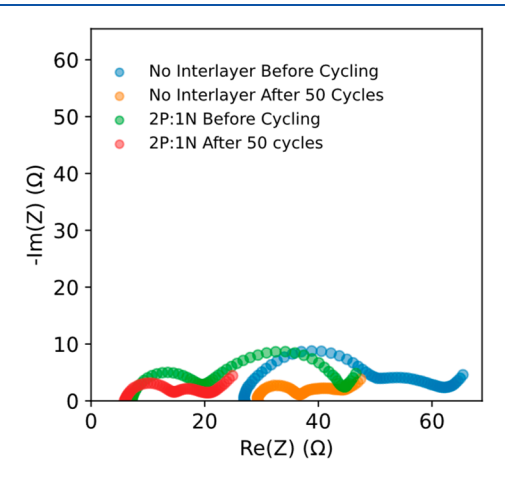


Figure 4. EIS of coin cells with and without the 2:1 interlayer before cycling and after 50 cycles.

To determine the impact of the interlayers on the specific capacity, we tested them in full Li-S coin cells. In the cycling data, the 3P:1N interlayer exhibited lower capacity and higher polarization than the 2P:1N interlayer in the Li-S coin cells, despite performing better in the Li-Li symmetric cells (Figure 5a,b). This is potentially due to increased polysulfide entrapment by smaller pores in the higher polymer ratio (denser) interlayer. Additionally, the gel state of a denser polymer matrix (after the interlayer swells with the liquid electrolyte) has also been found to physically trap polysulfides to some degree.<sup>23</sup> Note that the trapping effect is unlikely to come from functional groups in the polymer because there is little effect from the fluorine on polysulfides.<sup>23</sup> While polysulfide confinement in small pores and denser networks is known to be a desirable phenomenon on the cathode side, <sup>29,30</sup> we believe it is detrimental on the anode side. The larger pores and more open structure in the 2P:1N interlayer

would possibly allow any polysulfides that have migrated to the anode to shuttle back more freely to the cathode side.

Figure 5c compares the capacity between a cell with only Celgard and a cell with a 2P:1N interlayer. Because of the high porosity of the CNF cathode, we hypothesize that local liquid electrolyte availability could have been limited in some areas of the cathode. The addition of the interlayer heightens this effect. This may help explain the lower initial capacity and capacity rise as the components of the cell were being wetted and activated, and the sulfur was becoming redistributed and more accessible. 24,25 Additionally, the initial drop in capcity is due to the increase in cycling rate to C/2 after two formation cycles each at C/10 and C/5 rate. We believe there was a greater capacity increase in cells with the interlayer because the interlayer with LiNO3 could help PVDF-HFP to form LiF in a more robust SEI. This would reduce the reactivity of the lithium with polysulfides. LiNO3 has also been found to passivate the highly reactive lithium anode and inhibit it from reacting with polysulfides in the electrolyte.<sup>26</sup> The presence of LiNO<sub>3</sub> directly on the anode could be greatly heightening the protective effect that LiNO3 normally provides as a liquid electrolyte additive. Furthermore, we used post-mortem XPS to confirm the presence of LiNO<sub>3</sub> on the lithium surface in cells with the 2P:1N interlayer. Here, we observed the LiNO<sub>3</sub> peak at around 405 eV in the N 1s spectrum (Figure S2a) that was not present in cells without the interlayer. This is another observation that supports the idea that the CNF cathode takes up and retains a majority of the liquid electrolyte, preventing the full dissolution of the LiNO<sub>3</sub> in the interlayer.

After about 50 cycles, the capacity of each of the cells reached its maximum. We believe that at this point the sulfur was sufficiently redistributed, and the interlayer components were activated, which corresponds with the reduced cell resistance we observed with EIS (Figure 4). Although we detected lithium nitrate in the interlayer, some of the LiNO<sub>3</sub>

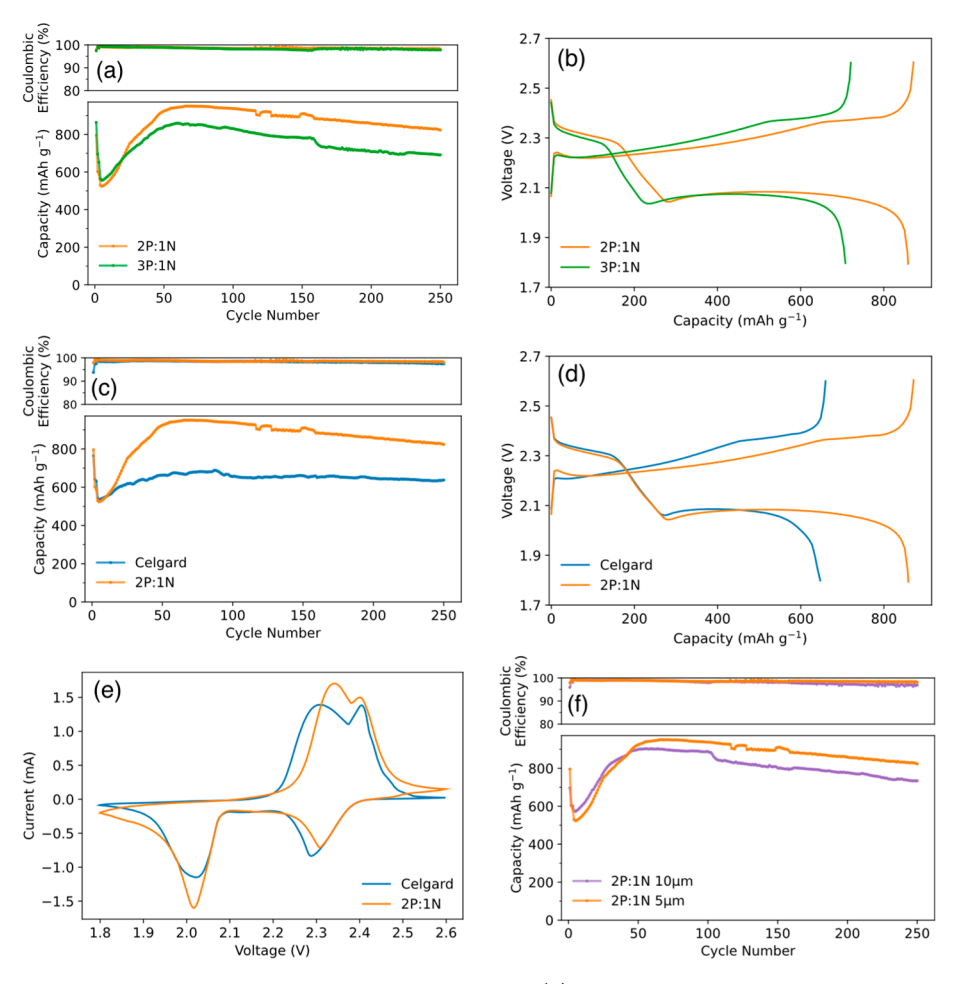


Figure 5. (a) Comparison of 2P:1N and 3P:1N interlayers in Li–S coin cells (b) and the corresponding voltage curves for the 200th cycle. (c) Comparison of coin cells with Celgard only and with the addition of a 2P:1N interlayer (d) and the corresponding voltage curve for the 200th cycle. (e) CV of a Celgard and 2P:1N interlayer cell. (f) Coin cells with 5 and 10  $\mu$ m thick 2P:1N interlayers.

may dissociate and increase the ionic conductivity in the cell. This may also reduce the resistance in the cell and help improve the conversion of polysulfides to Li<sub>2</sub>S<sub>2</sub> and Li<sub>2</sub>S in the 2P:1N interlayer cell. The decrease in resistance is also evidenced by a smaller polarization and a longer 2.1 V plateau in the corresponding voltage curve (Figure 5d). The kinetic behavior of the conversion reaction is reflected in the CV plots for these two cells (Figure 5e). Overall, the Celgard cell capacity remained fairly stable, providing 647 mAh g<sup>-1</sup> at cycle 200. However, its capacity was not as high as the 2P:1N interlayer cell, which provided 858 mAh g<sup>-1</sup> at cycle 200, a 32.6% increase in capacity over Celgard cells. The physical polysulfide trapping phenomenon could explain the gradual capacity fade. This same effect is seen in the 10  $\mu$ m thick 2P:1N interlayer cell (Figure 5f), which would have more pores than in a 5  $\mu$ m thick interlayer. This suggests that too thick of a layer would trap too many polysulfides.

**3.3.** XPS Analysis of Lithium Anode SEI. To investigate the effect of LiNO<sub>3</sub> in the interlayer, we gathered post-mortem XPS spectra of the lithium anode from lithium—sulfur coin cells that had interlayers with and without LiNO<sub>3</sub>. We compared these to a cell without any interlayer. In these experiments, we used a commercial ether electrolyte with its predetermined lithium salts to study the effect under more realistic electrolyte conditions. Figure 6a is the F 1s spectrum of a cell with an interlayer composed of only PVDF—HFP

(without LiNO<sub>3</sub>). It shows a smaller LiF peak relative to the C-F peak, which indicates that a small proportion of PVDF-HFP was converted to LiF. The relative peak ratio between the C-F and LiF peaks is 89.6% to 10.4%, respectively. Figure 6b shows the F 1s spectrum of a coin cell with the 2P:1N interlayer. Here, the LiF peak is much larger than the C-F peak. In this cell, the relative peak areas between the C-F and LiF are 33% to 66%. This suggests that the effect of LiNO<sub>3</sub> on the formation of LiF was significantly positive, even when commercial lithium salts were present in the liquid electrolyte. Finally, Figure 6c shows the F 1s spectra of a conventional lithium-sulfur coin cell with no interlayer. Here, the relative peak areas are nearly equal. However, there was no polymer interlayer that contributed to the C-F peak intensity. In the cell with the 2P:1N interlayer, the larger LiF peak highlights the extent of PVDF-HFP conversion to LiF. Therefore, we conclude that the increase in LiF in the 2P:1N interlayer cells is due to the presence of PVDF-HFP which reacts with lithium metal, and it is the addition of LiNO<sub>3</sub> that allows it to participate effectively in that reaction.

To further investigate the interfacial chemistry, we studied coin cells without lithium salts in the liquid electrolyte (DME:DOL 1:1 v:v). Still, in a coin cell with no fluorinated electrolyte salts, we detected LiF at 685 eV (Figure 6d). In this cell, the only source of fluorine was from the PVDF-HFP, indicating that the polymer undergoes a reaction with the

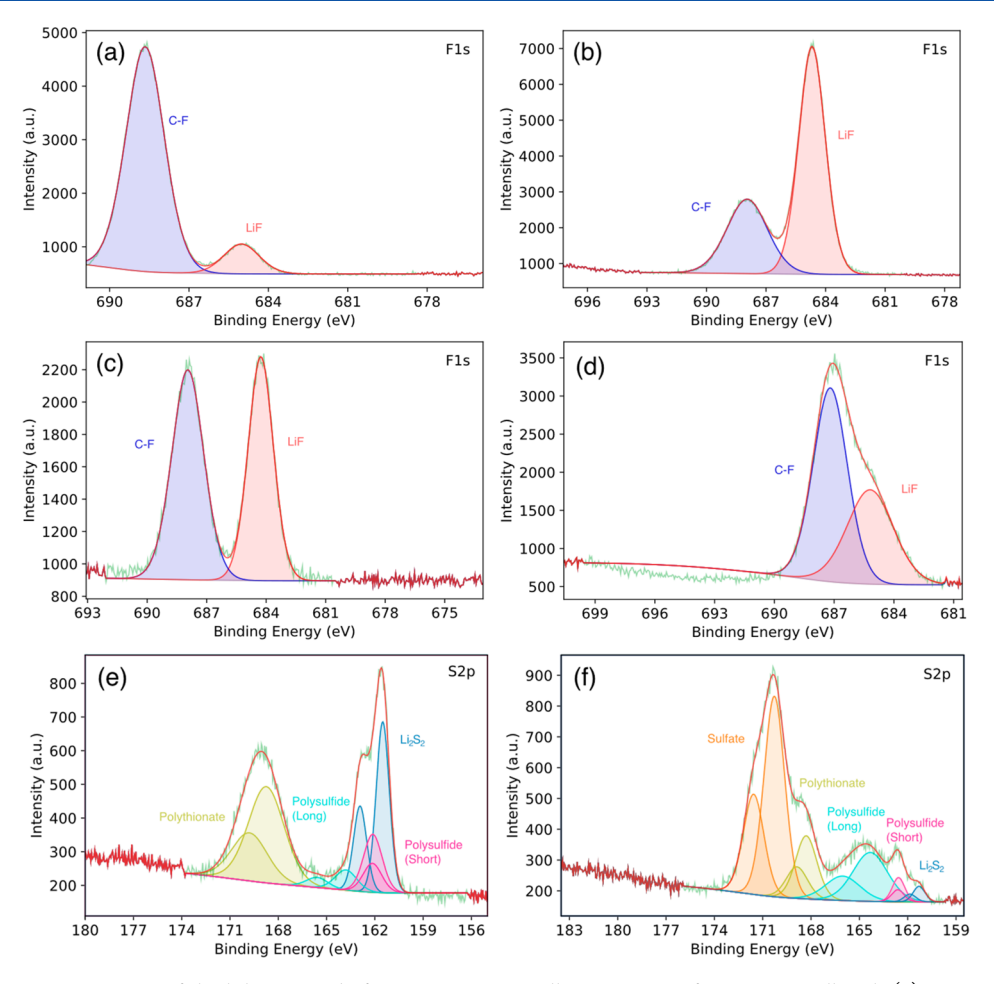


Figure 6. Post-mortem XPS spectra of the lithium anode from a Li–S coin cell. F 1s spectra from a coin cell with (a) an interlayer composed of only PVDF–HFP, (b) a 2P:1N interlayer, and (c) no interlayer. (d) F 1s spectrum of a Li–S coin cell with a 2P:1N interlayer and a liquid electrolyte composed of only 1:1 DME:DOL by volume (no LiTFSI). (e) S 2p spectra from a coin cell with no interlayer and (f) a coin cell with a 2P:1N interlayer.

lithium metal to form LiF. This agrees with findings from Guo et al., where their density functional theory (DFT) calculations showed that the reactants of this reaction have a higher energy than the products. This shows that the reaction between PVDF-HFP and lithium is favorable and forms LiF, hydrogen (H<sub>2</sub>), and PVDF-HFP-olefin. In their study, they performed this reaction ex situ and described the importance of a solvent, DMF. They proposed that electron-rich oxygen and nitrogen atoms in DMF were critical to this reaction. By placing the PVDF-HFP interlayer in the battery, we hypothesized that LiF forms in situ. In our system, the reaction may be aided by electron-donating groups, such as the ether electrolyte and other reduced species that have already reacted with the lithium metal. Furthermore, Li<sub>2</sub>O was also detected at 528 eV, which we expect is largely from the decomposition of the LiNO<sub>3</sub> salt (Figure S3).<sup>27</sup> This additional SEI component is a further advantage of this system.

Finally, we analyzed the post-mortem S 2p XPS spectra from coin cells with and without the 2P:1N interlayer. In the cell with the interlayer, prominent sulfate peaks appear at around 170 eV that are not present in cells without the interlayer (Figure 6e,f). This suggests that the lithium nitrate was acting as an oxidizer in the interlayer because it likely oxidized polysulfides into the  $\text{LiS}_x\text{O}_y$  sulfate species. Although, this effect in tandem with the polysulfide trapping behavior could simultaneously explain the very gradual decline in capacity over

time seen in the galvanostatic cycling plots. In addition to the lithium nitrate helping to decompose the PVDF–HFP, we suspect that these sulfates could also have promoted the breaking of the –CF $_3$  bond in PVDF–HFP to help form LiF, similar to how it does for LiTFSI, as Cheng et al. found in their work. <sup>28</sup> Furthermore, these  $\text{LiS}_x\text{O}_y$  species are ionically conductive and are beneficial to the SEI composition and its creation.

#### 4. CONCLUSION

In this work, a facile polymer and lithium salt interlayer was studied. In a Li–Li symmetric cell, the 3P:1N polymer electrolyte showed the highest stability. However, in a Li–S coin cell, the 2P:1N interlayer showed the best performance. We hypothesize that this is due to a physical polysulfide trapping phenomenon, relative to the density of the polymer networks. A Li–S coin cell with the 2P:1N interlayer saw a 32% capacity increase compared to cells without any interlayer after 200 cycles. The improved performance in symmetric and Li–S coin cells is likely due to the synergy between PVDF–HFP and LiNO<sub>3</sub> which resulted in the formation of higher amounts of LiF than in conventional cells. This was demonstrated via a series of post-mortem XPS measurements of lithium anodes from cycled cells. We hypothesized that the oxidative nature of LiNO<sub>3</sub> facilitated the breakdown of

PVDF—HFP to form LiF. Additionally, we believe that LiNO<sub>3</sub> also oxidized sulfur compounds to form sulfates that further facilitated the breakdown of PVDF—HFP. Finally, the process used to create this interlayer was simple and represents a step toward lowering industrial adoption barriers for lithium stability technologies.

## ASSOCIATED CONTENT

# **Solution** Supporting Information

The Supporting Information is available free of charge at https://pubs.acs.org/doi/10.1021/acsaem.3c02103.

Additional SEM images, post-mortem XPS spectra, and electrochemical data (PDF)

## AUTHOR INFORMATION

#### **Corresponding Author**

Vibha Kalra – Department of Chemical and Biological Engineering, Drexel University, Philadelphia, Pennsylvania 19104, United States; orcid.org/0000-0002-2630-1560; Email: vk99@drexel.edu

#### **Authors**

- Taber Yim Department of Chemical and Biological Engineering, Drexel University, Philadelphia, Pennsylvania 19104, United States
- Rhyz Pereira Department of Chemical and Biological Engineering, Drexel University, Philadelphia, Pennsylvania 19104, United States
- Neal Cardoza Department of Chemical and Biological Engineering, Drexel University, Philadelphia, Pennsylvania 19104, United States

Complete contact information is available at: https://pubs.acs.org/10.1021/acsaem.3c02103

#### Notes

The authors declare no competing financial interest.

# ACKNOWLEDGMENTS

This work was funded by the National Science Foundation (2211049, 1919177). We also acknowledge the staff members at the Materials Characterization Core (MCC) at Drexel University for their assistance and instrument time.

## REFERENCES

- (1) Pan, H.; Cheng, Z.; He, P.; Zhou, H. A Review of Solid-State Lithium-Sulfur Battery: Ion Transport and Polysulfide Chemistry. *Energy Fuels* **2020**, *34* (10), 11942–11961.
- (2) Pei, A.; Zheng, G.; Shi, F.; Li, Y.; Cui, Y. Nanoscale Nucleation and Growth of Electrodeposited Lithium Metal. *Nano Lett.* **2017**, *17* (2), 1132–1139.
- (3) Kim, H.; Jeong, G.; Kim, Y. U.; Kim, J. H.; Park, C. M.; Sohn, H. J. Metallic anodes for next generation secondary batteries. *Chem. Soc. Rev.* 2013, 42 (23), 9011–9034.
- (4) Wood, K. N.; Kazyak, E.; Chadwick, A. F.; Chen, K. H.; Zhang, J. G.; Thornton, K.; Dasgupta, N. P. Dendrites and Pits: Untangling the Complex Behavior of Lithium Metal Anodes through Operando Video Microscopy. ACS Cent Sci. 2016, 2 (11), 790–801.
- (5) Hong, H.; Che Mohamad, N. A. R.; Chae, K.; Marques Mota, F.; Kim, D. H. The lithium metal anode in Li-S batteries: challenges and recent progress. *J. Mater. Chem. A* **2021**, *9* (16), 10012–10038.
- (6) Aurbach, D.; Pollak, E.; Elazari, R.; Salitra, G.; Kelley, C. S.; Affinito, J. On the Surface Chemical Aspects of Very High Energy Density, Rechargeable Li-Sulfur Batteries. *J. Electrochem. Soc.* **2009**, 156 (8), A694.

- (7) Li, W.; Yao, H.; Yan, K.; Zheng, G.; Liang, Z.; Chiang, Y. M.; Cui, Y. The synergetic effect of lithium polysulfide and lithium nitrate to prevent lithium dendrite growth. *Nat. Commun.* **2015**, *6*, 7436.
- (8) Zu, C.; Dolocan, A.; Xiao, P.; Stauffer, S.; Henkelman, G.; Manthiram, A. Breaking Down the Crystallinity: The Path for Advanced Lithium Batteries. *Adv. Energy Mater.* **2016**, DOI: 10.1002/aenm.201501933.
- (9) Qian, J.; Henderson, W. A.; Xu, W.; Bhattacharya, P.; Engelhard, M.; Borodin, O.; Zhang, J. G. High rate and stable cycling of lithium metal anode. *Nat. Commun.* **2015**, *6*, 6362.
- (10) Qian, J.; Jin, B.; Li, Y.; Zhan, X.; Hou, Y.; Zhang, Q. Research progress on gel polymer electrolytes for lithium-sulfur batteries. *Journal of Energy Chemistry* **2021**, *56*, 420–437.
- (11) Guo, S.; Piao, N.; Wang, L.; Xu, H.; Tian, G.; Li, J.; He, X. PVDF-HFP/LiF Composite Interfacial Film to Enhance the Stability of Li-Metal Anodes. ACS Applied Energy Materials 2020, 3 (7), 7191–7199
- (12) Zhao, K.; Jin, Q.; Zhang, L.; Li, L.; Wu, L.; Zhang, X. Achieving dendrite-free lithium deposition on the anode of Lithium-Sulfur battery by LiF-rich regulation layer. *Electrochim. Acta* **2021**, 393, 138981.
- (13) Dong, Q.; Hong, B.; Fan, H.; Jiang, H.; Zhang, K.; Lai, Y. Inducing the Formation of In Situ Li3N-Rich SEI via Nanocomposite Plating of Mg3N2 with Lithium Enables High-Performance 3D Lithium-Metal Batteries. ACS Appl. Mater. Interfaces 2020, 12 (1), 627–636.
- (14) Zhang, J.; Sun, B.; Huang, X.; Chen, S.; Wang, G. Honeycomblike porous gel polymer electrolyte membrane for lithium ion batteries with enhanced safety. *Sci. Rep* **2014**, *4*, 6007.
- (15) Polat, K. Energy harvesting from a thin polymeric film based on PVDF-HFP and PMMA blend. *Appl. Phys. A: Mater. Sci. Process.* **2020**, DOI: 10.1007/s00339-020-03698-w.
- (16) Ruiz, M. L.; Lick, I. D.; Ponzi, M. I.; Castellón, E. R.; Jiménez-López, A.; Ponzi, E. N. Thermal decomposition of supported lithium nitrate catalysts. *Thermochim. Acta* **2010**, 499 (1–2), 21–26.
- (17) Liu, H.; Cheng, X. B.; Xu, R.; Zhang, X. Q.; Yan, C.; Huang, J. Q.; Zhang, Q. Plating/Stripping Behavior of Actual Lithium Metal Anode. *Adv. Energy Mater.* **2019**, DOI: 10.1002/aenm.201902254.
- (18) Waluś, S.; Barchasz, C.; Bouchet, R.; Alloin, F. Electrochemical impedance spectroscopy study of lithium-sulfur batteries: Useful technique to reveal the Li/S electrochemical mechanism. *Electrochim. Acta* **2020**, *359*, 136944.
- (19) Choi, W.; Shin, H.-C.; Kim, J. M.; Choi, J.-Y.; Yoon, W.-S. Modeling and Applications of Electrochemical Impedance Spectroscopy (EIS) for Lithium-ion Batteries. *Journal of Electrochemical Science and Technology* **2020**, *11* (1), 1–13.
- (20) Fu, J.; Ji, X.; Chen, J.; Chen, L.; Fan, X.; Mu, D.; Wang, C. Lithium Nitrate Regulated Sulfone Electrolytes for Lithium Metal Batteries. *Angew. Chem., Int. Ed. Engl.* **2020**, 59 (49), 22194–22201.
- (21) Chiu, L.-L.; Chung, S.-H. Composite gel-polymer electrolyte for high-loading polysulfide cathodes. *J. Mater. Chem. A* **2022**, *10* (26), 13719–13726.
- (22) Yu, X.; Pan, H.; Zhou, Y.; Northrup, P.; Xiao, J.; Bak, S.; Liu, M.; Nam, K.-W.; Qu, D.; Liu, J.; Wu, T.; Yang, X.-Q. Direct Observation of the Redistribution of Sulfur and Polysufides in Li-S Batteries During the First Cycle by In Situ X-Ray Fluorescence Microscopy. *Adv. Energy Mater.* **2015**, DOI: 10.1002/aenm.201500072.
- (23) Yang, Q.; Deng, N.; Chen, J.; Cheng, B.; Kang, W. The recent research progress and prospect of gel polymer electrolytes in lithium-sulfur batteries. *Chemical Engineering Journal* **2021**, 413, 127427.
- (24) Cui, C.; Zhang, R.; Fu, C.; Xie, B.; Du, C.; Wang, J.; Gao, Y.; Yin, G.; Zuo, P. Stabilizing Lithium Metal Anode Enabled by a Natural Polymer Layer for Lithium-Sulfur Batteries. *ACS Appl. Mater. Interfaces* **2021**, *13* (24), 28252–28260.
- (25) Chung, S. H.; Chang, C. H.; Manthiram, A. A Carbon-Cotton Cathode with Ultrahigh-Loading Capability for Statically and Dynamically Stable Lithium-Sulfur Batteries. *ACS Nano* **2016**, *10* (11), 10462–10470.

- (26) Liang, X.; Wen, Z.; Liu, Y.; Wu, M.; Jin, J.; Zhang, H.; Wu, X. Improved cycling performances of lithium sulfur batteries with LiNO3-modified electrolyte. *J. Power Sources* **2011**, *196* (22), 9839–9843.
- (27) Adams, B. D.; Carino, E. V.; Connell, J. G.; Han, K. S.; Cao, R.; Chen, J.; Zheng, J.; Li, Q.; Mueller, K. T.; Henderson, W. A.; Zhang, J.-G. Long term stability of Li-S batteries using high concentration lithium nitrate electrolytes. *Nano Energy* **2017**, *40*, 607–617.
- (28) Cheng, X.-B.; Yan, C.; Chen, X.; Guan, C.; Huang, J.-Q.; Peng, H.-J.; Zhang, R.; Yang, S.-T.; Zhang, Q. Implantable Solid Electrolyte Interphase in Lithium-Metal Batteries. *Chem.* **2017**, 2 (2), 258–270.
- (29) Singhal, R.; Chung, S.-H.; Manthiram, A.; Kalra, V. A free-standing carbon nanofiber interlayer for high-performance lithium—sulfur batteries. *J. Mater. Chem. A* **2015**, 3 (8), 4530–4538.
- (30) Chung, S.-H.; Singhal, R.; Kalra, V.; Manthiram, A. Porous Carbon Mat as an Electrochemical Testing Platform for Investigating the Polysulfide Retention of Various Cathode Configurations in Li-S Cells. J. Phys. Chem. Lett. 2015, 6 (12), 2163–2169.